On the use of Pseudo-Noise Ranging with high-rate spectrally-efficient modulations

SpaceOps-2021,8,x1605

On the use of PN Ranging with High-rate Spectrally-efficient Modulations

B. Ripani[a,*], A. Modenini[b], R. Garello[a], G. Maiolini Capez[a], and G. Montorsi[a]

[a] *Politecnico di Torino, Corso Duca degli Abruzzi 24, Torino, Italy*
{barbara.ripani, roberto.garello, gabriel.maiolinicapez, guido.montorsi}@polito.it
[b] *European Space Agency, Keplerlaan 1, Noordwijk, The Netherlands*
andrea.modenini@esa.int
[*] Corresponding Author

Abstract

In this paper, we study the feasibility of coupling the PN ranging with filtered high-order modulations, and investigate the simultaneous demodulation of a high-rate telemetry stream while tracking the PN ranging sequence. Accordingly, we design a receiver scheme that is able to perform a parallel cancellation, in closed-loop, of the ranging and the telemetry signal reciprocally. From our analysis, we find that the non-constant envelope property of the modulation causes an additional jitter on the PN ranging timing estimation that, on the other hand, can be limited by properly sizing the receiver loop bandwidth.

Our study proves that the use of filtered high-order modulations combined with PN ranging outperforms the state-of-the-art in terms of spectral efficiency and achievable data rate, while having comparable ranging performance.

Keywords: PN Ranging, GMSK, high-order modulations, SRS, Chip tracking loop.

1 Introduction

Space agencies are currently replacing transparent ranging systems with regenerative schemes to meet future Space Research (SR) mission needs. For this purpose, the Consultative Committee for Space Data Systems (CCSDS) defined the Pseudo-Noise (PN, [1, 2]) ranging standard, a state-of-the-art positioning technique. This standard, already implemented in the ESA missions BepiColombo and Solar Orbiter, demonstrated an accuracy as high as a few centimetres during its validation [3, 4]. Additionally, the possibility of coupling the PN ranging with a Gaussian Minimum Shift Keying (GMSK, [5]) modulated signal allows simultaneous reception of high-rate telemetry streams and orbit determination.

However, Near Earth SR missions transmitting telemetry in X-Band, in agreement with frequency assignment regulations [6], are constrained to 10 MHz of bandwidth. Thus, when using GMSK, these missions are limited to a data rate of 8.7 Mbps, penalizing payload data generation (see the case of GAIA mission [7]). To exceed this bound, it is clear that high-order modulation schemes must be adopted. However, their compatibility with PN ranging (to the best of the authors' knowledge) was never investigated.

In this paper, we study the coupling of PN ranging with filtered (amplitude) Phase-Shift Keying (PSK/APSK) signals, by taking the CCSDS standard 131.2 [8, 9] as a reference. Namely, we define a receiver scheme that is able to simultaneously demodulate the PSK/APSK stream, with modulation orders as high as 64, and track the PN ranging sequence. This is done by performing a parallel closed-loop cancellation of the PN ranging sequence over the telemetry symbols and vice-versa. To evaluate the performance of the system we designed, we assess both the Bit Error Rate (BER) and the ranging timing jitter, revealing the presence of a noise floor due to the non-constant envelope of PSK/APSK modulations. By modeling this phenomenon we derive a closed-form expression that constitutes an upper-bound for the ranging jitter.

In this work, we find the performance of the proposed scheme to be comparable to the classical GMSK approach, while enabling much higher data rates, thus paving the way towards a new generation of SR missions with more ambitious scientific objectives.

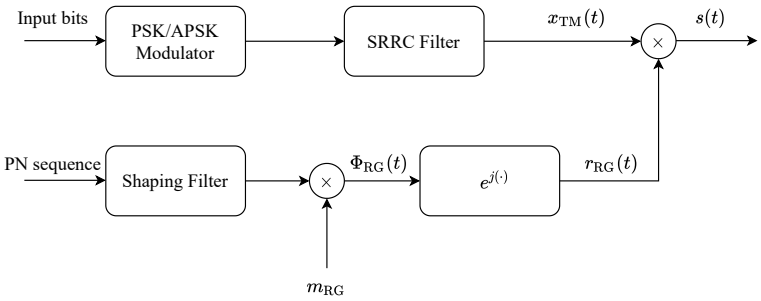

Figure 1: Transmitter block diagram.

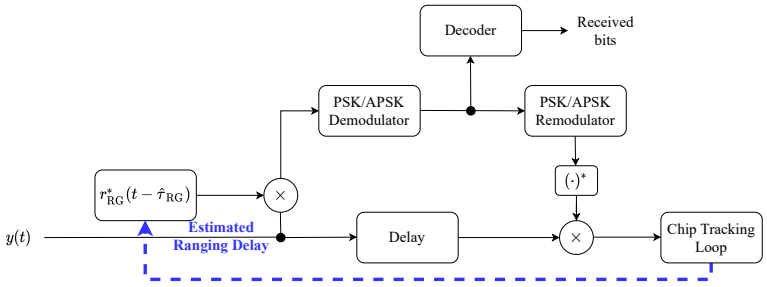

Figure 2: Receiver block diagram.

2 System Model

We consider the transmission system described by the block diagram reported in Figure 1. The complex baseband modulated telemetry signal, with unitary power, is defined as

$$x_{\mathrm{TM}}(t) = \sum_k a_k p(t - kT)\,, \tag{1}$$

where $p(t)$ is the Square Root Raised Cosine (SRRC) shaping pulse, and $\{a_k\}$ the sequence of telemetry symbols, each transmitted at symbol time kT, and belonging to a complex PSK/APSK constellation. Instead, the phase-modulated ranging signal $r_{\mathrm{RG}}(t)$ is defined as $r_{\mathrm{RG}}(t) = e^{j\Phi_{\mathrm{RG}}(t)}$ and its phase can be expressed as

$$\Phi_{\mathrm{RG}}(t) = m_{\mathrm{RG}} \sum_k c_k h(t - kT_c)\,, \tag{2}$$

where m_{RG} is the ranging modulation index, $h(t)$ the sinusoidal chip shaping pulse defined in [1], and $\{c_k\}$ the sequence of chips transmitted at chip time kT_c. Note that, in line with CCSDS recommendation 2.4.22A [10], we imposed $T_c \neq nT$, with $n \in \mathbb{Z}^+$.

Therefore, by considering a transmission over the Additive White Gaussian Noise (AWGN) channel, the received signal reads

$$y(t) = x_{\mathrm{TM}}(t) \cdot r_{\mathrm{RG}}(t - \tau_{\mathrm{RG}}) + w(t)\,, \tag{3}$$

where $w(t)$ is white Gaussian noise with spectral density equal to N_0 and $\tau_{\mathrm{RG}} \in [-\frac{T_c}{2}, \frac{T_c}{2})$ is an arbitrary ranging timing delay.

3 Receiver for PSK/APSK-modulated signals and PN Ranging

We implement a modified version of the receiver defined in [11] that performs parallel closed-loop cancellation of telemetry and ranging signals from the received stream. The receiver's block diagram is shown in Figure 2.

The ranging component is removed from the received signal by using a locally generated replica of the ranging signal. Mathematically,

$$y(t) r^*_{\mathrm{RG}}(t - \hat{\tau}_{\mathrm{RG}}) = x_{\mathrm{TM}}(t) + w(t) r^*_{\mathrm{RG}}(t - \hat{\tau}_{\mathrm{RG}})\,, \tag{4}$$

being $r^*_{\mathrm{RG}}(t)$ the ranging signal's complex conjugate, locally generated using the estimated time delay $\hat{\tau}_{\mathrm{RG}}$. It is easy to see that, being $r_{\mathrm{RG}}(t)$ a phasor, the resultant process $w(t) r^*_{\mathrm{RG}}(t - \hat{\tau}_{\mathrm{RG}})$ is still white Gaussian, and $x_{\mathrm{TM}}(t)$ is perfectly recovered as long as $\hat{\tau}_{\mathrm{RG}} = \tau_{\mathrm{RG}}$, since $|r_{\mathrm{RG}}(t - \tau_{\mathrm{RG}})|^2 = 1$. The telemetry stream thus obtained is demodulated to extract data, and then re-modulated to obtain the sequence of symbols. With it,

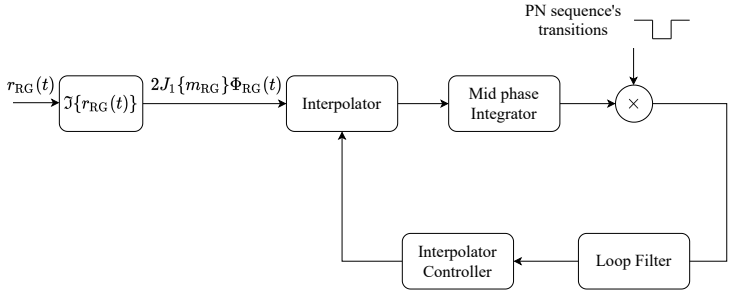

Figure 3: Chip tracking loop block diagram.

Table 1: Telemetry power variance σ_P^2 for different PSK/APSK modulations and roll-off factors.

Roll-off	QPSK	8-PSK	16-APSK	32-APSK	64-APSK
0.2	0.240	0.243	0.435	0.560	0.483
0.25	0.224	0.226	0.426	0.554	0.474
0.3	0.209	0.211	0.418	0.551	0.467
0.35	0.197	0.199	0.412	0.549	0.462

we generate the complex conjugate $x^*_{\mathrm{TM}}(t)$, necessary to sub-optimally cancel the telemetry component from the received signal. We can write

$$y(t)x^*_{\mathrm{TM}}(t) = r_{\mathrm{RG}}(t-\tau_{\mathrm{RG}})|x_{\mathrm{TM}}(t)|^2 + \mathcal{W}(t)\,, \tag{5}$$

where $\mathcal{W}(t) = x^*_{\mathrm{TM}}(t)w(t)$ can be proved[1] to be a white process with power spectral density equal to N_0. Since $x_{\mathrm{TM}}(t)$ is SRRC filtered, $|x_{\mathrm{TM}}(t)|^2 \neq 1$, and thus perfect cancellation cannot be achieved. However, taking into account that $\mathbb{E}[|x_{\mathrm{TM}}(t)|^2] = 1$, sub-optimal cancellation can be performed by averaging the samples of the telemetry signal's time-varying envelope, as shown in Section 4.

Once recovered, the ranging sequence is input to the Chip Tracking Loop (CTL), whose block diagram is depicted in Figure 3. Since the ranging chip sequence resembles a clock signal, we implement the CTL as a modified version of the Data Transition Tracking Loop (DTTL) [2, 13]. In this case, the mid-phase integrator operates according to an Integrate and Dump approach, integrating the PN sequence over a time interval T_c between two consecutive chips. Then, the mid-phase integrator output is multiplied by the PN transition sequence to adjust the sign of the error at the input of the loop filter.

Finally, the estimated CTL timing $\hat{\tau}_{\mathrm{RG}}$ is fed back to the local PN generator in Figure 2, thus closing the receiver loop.

4 Ranging Timing Jitter

In this section we analyze the timing jitter of the receiver scheme presented in Section 3.

We define $\mathcal{P}(t) = |x_{\mathrm{TM}}(t)|^2 - 1$ as a zero-mean signal with variance $\sigma_P^2 = \mathbb{E}[|x_{\mathrm{TM}}(t)|^2]$, which depends on the adopted telemetry modulation and is equal to the values reported in Table 1.

Thus, Equation (5) can be re-written as

$$y(t)x^*_{\mathrm{TM}}(t) = r_{\mathrm{RG}}(t-\tau_{\mathrm{RG}}) + \mathcal{W}(t) + r_{\mathrm{RG}}(t-\tau_{\mathrm{RG}})\mathcal{P}(t)\,, \tag{6}$$

where the last term can be understood as additional noise arising from the non-constant envelope of the considered modulation formats. To assess its impact, we analyze the output of the CTL. As Figure 3 shows, the CTL extracts the imaginary component of the ranging signal, which reads

$$\alpha\Phi_{\mathrm{RG}}(t-\tau_{\mathrm{RG}}) + \mathcal{N}(t) + \mathcal{D}(t)\,, \tag{7}$$

where $\mathcal{N}(t)$ is the imaginary component of the Gaussian noise, $\mathcal{D}(t) = \alpha\Phi_{\mathrm{RG}}(t-\tau_{\mathrm{RG}})\mathcal{P}(t)$, and[2] $\alpha \approx 2J_1(m_{\mathrm{RG}})$.

Therefore, we define $n \triangleq \int_0^{T_c} \mathcal{N}(t)\,\mathrm{d}t$ and $\zeta \triangleq \int_0^{T_c} \mathcal{D}(t)\,\mathrm{d}t$, i.e, the output of the mid-phase integrator when $\mathcal{N}(t)$ and $\mathcal{D}(t)$ are input, respectively. While it is easy to see that $\mathbb{E}[|n|^2] = T_c N_0$, a closed-form solution for

[1] It is pointed out that the signal $x_{\mathrm{TM}}(t)$ is actually a cyclostationary process, thus making $\mathcal{W}(t)$ cyclostationary as well. However, without loss of generality, in this paper we consider their stationary statistics by simply referring to the cyclic auto-correlation at null cyclic frequency [12].

[2] Considering sine-shaped chip pulses, applying the Jacobi-Anger expansion we have $r_{\mathrm{RG}}(t) \approx J_0(m_{\mathrm{RG}}) + j2J_1(m_{\mathrm{RG}})\Phi_{\mathrm{RG}}(t)$ [11].

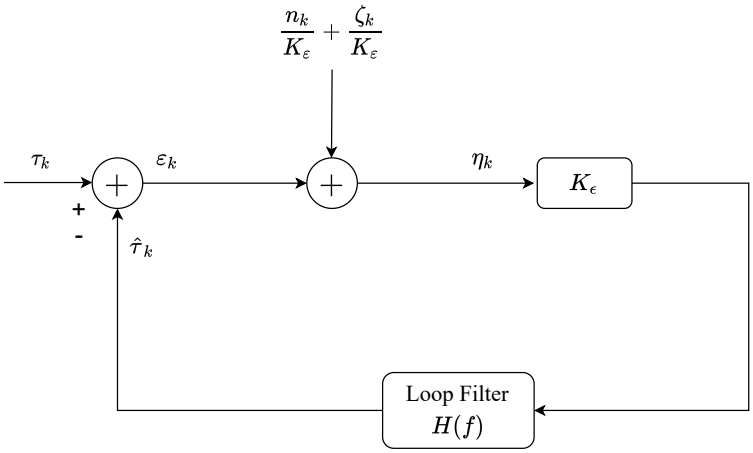

Figure 4: Linearized CTL model.

$\mathbb{E}[|\zeta|^2]$ is not easy to obtain but we derive its upper-bound. In fact, by considering that the auto-correlation of $\mathcal{D}(t)$ is always lower than $\mathbb{E}[|\mathcal{D}(t)|^2]$

$$\mathbb{E}[|\zeta|^2] \leq \int_0^{T_c} \int_0^{T_c} \mathbb{E}[|\mathcal{D}(t)|^2] \, \mathrm{d}t_1 \mathrm{d}t_2 = P\sigma_P^2 T_c^2 \,, \tag{8}$$

with $P = \mathbb{E}[|\alpha\Phi_{\mathrm{RG}}(t)|^2]$, i.e., the useful power of the received ranging signal at the input of the CTL.

We assume ζ to be a white process. Thus, we derive a linearized model of the CTL, as reported in Figure 4, in which both the discretized noise terms at the k-th time (n_k and ζ_k) are added to the phase detector output ε_k. The loop error is defined as

$$\eta_k = \varepsilon_k + \frac{n_k}{K_\varepsilon} + \frac{\zeta_k}{K_\varepsilon} \,, \tag{9}$$

where $K_\varepsilon = 2\sqrt{2P}$ is the mid-phase integrator gain [2].
Considering that n_k and ζ_k are uncorrelated, the loop error variance is $\sigma_\eta^2 = (\mathbb{E}[|n_k|^2] + \mathbb{E}[|\zeta_k|^2])/K_\varepsilon^2$. Thus, by using Equation (8), and filtering the loop error η_k through the Loop Filter with transfer function $H(f)$, the ranging timing variance is upper-bounded by

$$\sigma_\tau^2 \leq T_c \int_0^{1/T_c} \left| \frac{K_\varepsilon H(f)}{1 + K_\varepsilon H(f)} \right|^2 \cdot T_c \left(\frac{N_0}{8P} + \frac{\sigma_P^2 T_c}{8} \right) df \,. \tag{10}$$

Recalling the definition of the noise bandwidth B_L [14] from Equation (10) we obtain

$$\sigma_\tau^2 \leq B_L T_c^2 \left(\frac{N_0}{8P} + \frac{\sigma_P^2 T_c}{8} \right) . \tag{11}$$

It is interesting to observe that the first noise RHS term in Equation (11) coincides with the theoretical PN ranging jitter [2], and is reduced as $P/N_0 B_L$ grows. However, due to the modulation's non-constant envelope, the second RHS term appears. As it is directly proportional to the product $\sigma_P^2 B_L$, the only way to reduce this noise term is by narrowing the noise loop bandwidth B_L, i.e., by averaging the samples of the varying envelope.

5 Numerical Results

We simulate the transmission of a SRRC filtered telemetry signal, with channel symbol rate $R = 1/T = 4.2$ Msymbol/s, together with a PN ranging signal of rate $R_c = 1/T_c = 3$ Mchip/s.

First, we analyze the occupied bandwidth in an AWGN channel (as 99-percent of the signal power): in absence of ranging, the telemetry signal has approximately 4.8 MHz of bandwidth. Instead, in the presence of the PN signal, the spectral occupancy changes as a function of the ranging modulation index m_{RG} as shown in Table 2. For comparison, we include the bandwidth of a GMSK modulated signal (with the same bitrate of a QPSK modulated signal). It can be seen that, even in presence of ranging, PSK/APSK modulations are more spectrally-efficient than GMSK. Thus, when subject to spectral regrowth due to power amplification (not considered in this paper), the two schemes will have similar bandwidths.

Table 2: Occupied bandwidth for PSK/APSK (SRRC filtered with roll-off 0.35) and GMSK modulated telemetry, over the AWGN channel, as a function of the ranging modulation index m_{RG}.

m_{RG}	PSK/APSK	GMSK
0.111	4.87 MHz	7.22 MHz
0.222	5.04 MHz	7.31 MHz
0.444	6.38 MHz	7.72 MHz
0.666	7.31 MHz	8.23 MHz

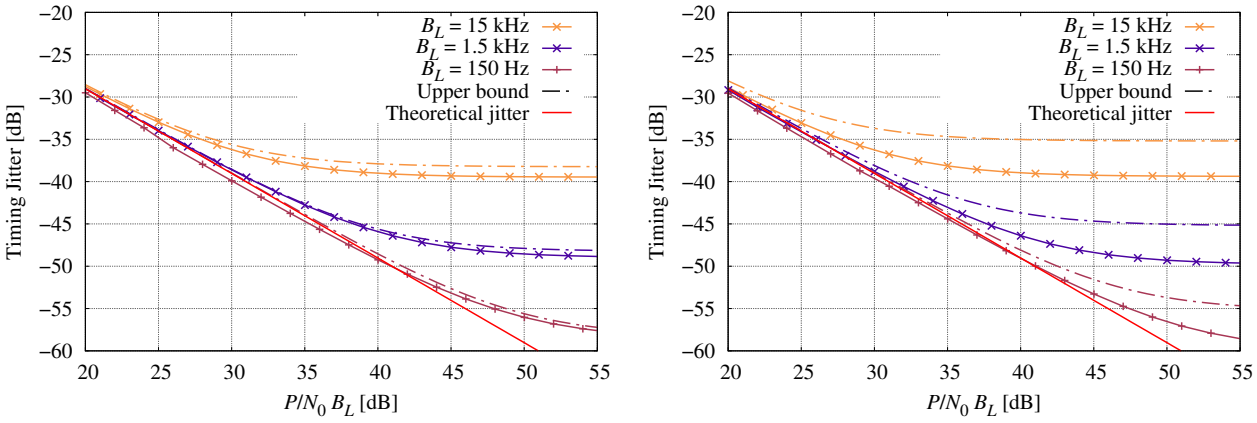

(a) QPSK

(b) 64-APSK

Figure 5: Impact of SRRC-filtered modulations on timing jitter in a genie-aided receiver (roll-off = 0.2).

Next, we analyze the ranging jitter in the ideal condition of perfectly demodulated telemetry symbols. To do so, we implement and simulate a genie-aided receiver that is provided with the correct sequence of symbols $\{a_k\}$. We evaluate the timing jitter σ_τ^2, normalized to T_c^2, as a function of the signal-to-noise ratio P/N_0B_L and for different values of B_L. Figure 5 shows the simulation results for SRRC filtered (roll-off = 0.2) QPSK (Figure 5a) and 64-APSK (Figure 5b) modulations. For comparison, the upper-bound of Equation (11) is shown together with the theoretical PN ranging jitter derived in [2]. As predicted, the jitter has a floor that decreases with B_L, and thus the performance gets closer to the theoretical jitter. In particular, a value $B_L = 150$ Hz provides almost ideal performance, without limiting the timing synchronization dynamic. Additionally, Figure 5 shows that as the modulation order decreases, the upper-bound is tighter to the actual jitter.

Finally, we evaluate the end-to-end performance of the receiver scheme of Figure 2 from the telemetry and ranging points of view, simulating the complete communication chain. Figure 6 and 7 present the ranging timing jitter and the telemetry's BER as a function of P/N_0B_L and E_b/N_0 (being E_b the energy per bit), respectively, for all SRRC-filtered PSK/APSK modulations (roll-off = 0.2). For the two modulation sets the same trend is observed: despite an initial deviation (more pronounced as the modulation order grows), the simulated ranging jitter curves (Figure 6a and 7a) coincide with the genie-aided curve, which is free of telemetry losses. Although the telemetry and ranging performances are inherently intertwined, the worsened jitter performance for low values of P/N_0B_L, with respect to ideal cancellation, is not reflected in the BER. In fact, the end-to-end BER is comparable to the modulations' theoretical performance in an AWGN channel in the absence of ranging. (Figure 6b and 7b).

6 Conclusions

In this paper, we investigated the possibility of combining the PN ranging with high-order, spectrally-efficient PSK/APKS modulations. At the receiver side, we designed, implemented and simulated a receiver scheme for simultaneous demodulation of high-order telemetry symbols and tracking of the received ranging sequence for orbit determination. The obtained results show that it is possible to achieve ranging performance comparable to current state-of-the-art receiver architecture by simply lowering the noise loop bandwidth B_L. Furthermore, the introduction of such modulations for combined telemetry and ranging more than doubles/triples the current data rate bound of 8.7 Mbps.

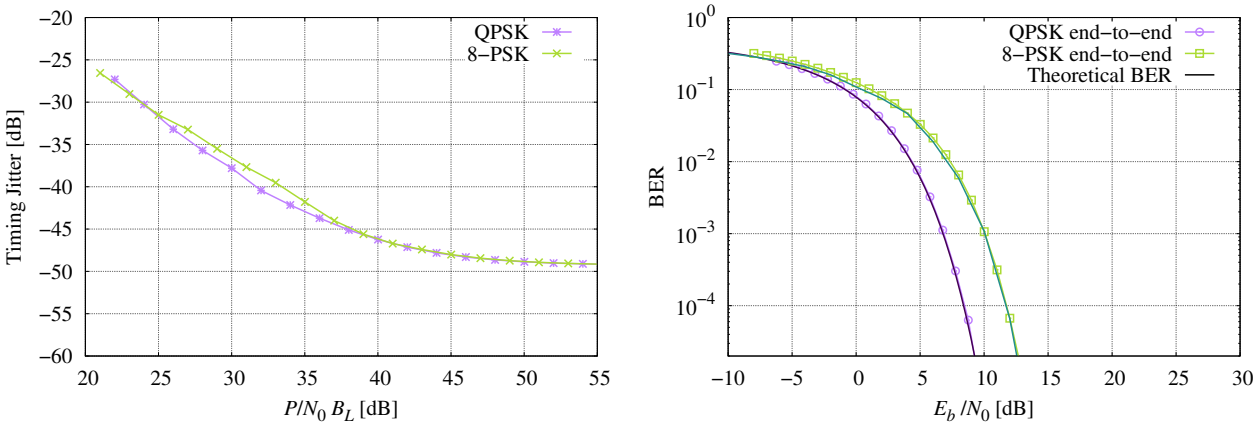

(a) Ranging timing jitter

(b) Telemetry BER

Figure 6: End-to-end ranging and telemetry performance for QPSK and 8-PSK modulations ($B_L = 1.5$ kHz).

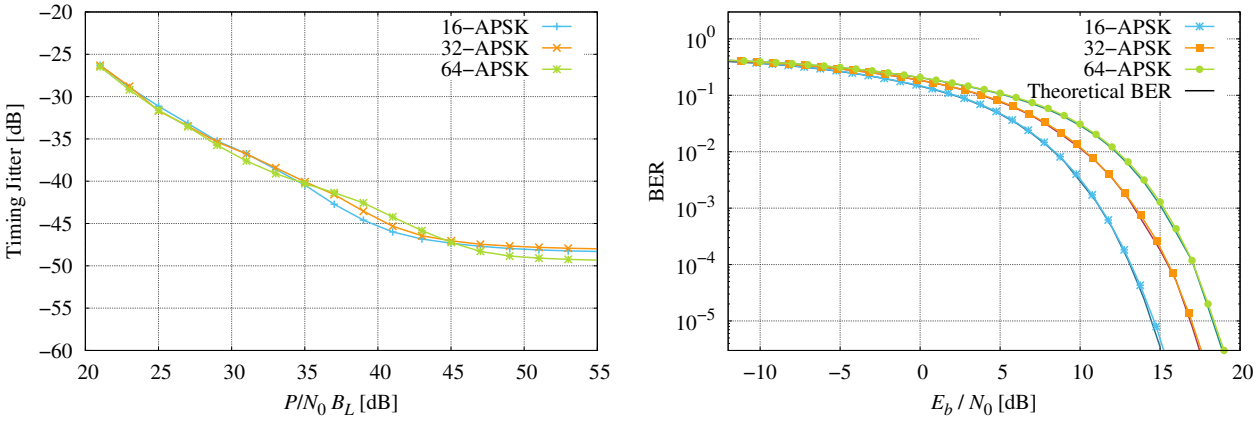

(a) Ranging Timing Jitter

(b) Telemetry BER

Figure 7: End-to-end ranging and telemetry performance for 16-APSK, 32-APSK, and 64-APSK modulations ($B_L = 1.5$ kHz).

Disclaimer

The view expressed herein can in no way be taken to reflect the official opinion of the European Space Agency.

References

[1] CCSDS 414.1-B-2, *Pseudo-Noise PN Ranging Systems*, 2014, Available at http://public.ccsds.org/.

[2] CCSDS 414.0-G-2, *Pseudo-Noise PN Ranging Systems*, 2014, Available at http://public.ccsds.org/.

[3] P. Cappuccio, V. Notaro, L. Iess, S. Asmar, J. Border, S. Ciarcia Sr, A. Di Ruscio, E. Montagnon, J. De Vicente, M. Mercolino *et al.*, "First results from cruise tests of the mercury orbiter radio science experiment (MORE) of ESA's BepiColombo mission," *AGUFM*, vol. 2019, pp. P34A–04, 2019.

[4] M. Mascarello, G. Sessler, E. Vassallo, G. R. Iglesias, K. Kewin, M. Montagna, and L. Manso, "The Solar Orbiter X-Band TT&C New Features: GMSK with PN Regenerative Ranging and DDOR Semaphores Implementation," in *2019 8th International Workshop on Tracking, Telemetry and Command Systems for Space Applications (TTC)*, 2019, pp. 1–6.

[5] K. Murota and K. Hirade, "GMSK modulation for digital mobile radio telephony," *IEEE Transactions on communications*, vol. 29, no. 7, pp. 1044–1050, 1981.

[6] Space Frequency Coordination Group, "Use of the 8450-8500 MHz band for space research, category A," 1998, REC SFCG 5-1R5.

[7] European Space Agency, "GAIA flight model payload data handling unit delivered and integrated," Available at https://sci.esa.int/web/gaia/-/51777-09-gaia-flight-model-payload-data-handling-unit-delivered-and-integrated .

[8] CCSDS 130.11-G-1, *SCCC—Summary of definition and performance*, 2019, Available at http://public.ccsds.org/.

[9] CCSDS 131.2-B-1, *Flexible advanced coding and modulation scheme for high rate telemetry applications*, 2012, Available at http://public.ccsds.org/.

[10] CCSDS 401.0-B-31, *Radio Frequency and modulation systems - Part 1 Earth Stations and Spacecrafts*, 2020, Available at http://public.ccsds.org/.

[11] CCSDS 413.1-G-1, *Simultaneous transmission of GMSK telemetry and PN Ranging*, 2017, Available at http://public.ccsds.org/.

[12] A. Papoulis, *Probability, Random Variables and Stochastic Processes*, New York, NY, 1991.

[13] Jet Propulsion Laboratory, California Institute of Technology, "Autonomous software-defined radio receivers for deep space applications," JPL, Tech. Rep., 2006.

[14] F. M. Gardner, *Phaselock techniques*. John Wiley & Sons, 2005.